


# SCIENTIFIC REPORTS

OPEN

## Effect of Substrate symmetry on the dendrite morphology of MoS<sub>2</sub> Film synthesized by CVD

Di Wu<sup>1</sup>, Tai Min<sup>1</sup>, Jian Zhou<sup>1</sup> , Chen Li<sup>2</sup>, Guobin Ma<sup>2</sup>, Gaotian Lu<sup>3</sup>, Minggang Xia<sup>1,4</sup> & Zhengbin Gu<sup>2</sup>

Received: 4 May 2017

Accepted: 20 September 2017

Published online: 09 November 2017

In van der Waals epitaxial growth, the substrate plays a particularly important role in the crystal morphology. Here, we synthesized MoS<sub>2</sub> by chemical vapour deposition on silicon carbide (SiC). The obtained MoS<sub>2</sub> dendritic crystals show six-fold symmetry, which are different from the conventional triangular shapes on SiO<sub>2</sub> substrate and from those with three-fold symmetry on SrTiO<sub>3</sub> substrate. Interestingly, these MoS<sub>2</sub> dendritic crystals on SiC exhibit an average fractal dimension 1.76, which is slightly larger than the classical Diffusion-limited-Aggregation fractal dimension 1.66. The first principle calculation indicates that the six-fold symmetry of the dendritic MoS<sub>2</sub> is determined by the lattice symmetry of SiC. To further demonstrating the substrate effect, we break the natural six-fold lattice symmetry of SiC (0001) into groove arrays through etching the substrate. And then we successfully synthesized cross-type dendritic crystal MoS<sub>2</sub> with two-fold symmetry. Its average fractal dimension 1.83 is slightly larger than the fractal dimension 1.76 of the previous MoS<sub>2</sub> dendrite with six-fold symmetry. In a word, the symmetry of SiC substrate determined the symmetry and the fractal dimension of the dendritic MoS<sub>2</sub>. This work provides one possibility of inducing the growth orientation of dendritic crystals through controlling the substrate surface symmetry artificially.

In the past ten years, two dimensional (2D) transition-metal dichalcogenides (TMDs) materials have received considerable research interests in many fields for their wide range of potential applications, including optoelectronic devices<sup>1-3</sup>, capacitors<sup>4</sup>, hydrogen storage<sup>5</sup>, catalysis<sup>6</sup>, and solid lubricant<sup>7</sup>, because of their unique electrical, chemical and mechanical properties. Among many transition-metal dichalcogenides, one of the most promising representatives is molybdenum disulfide (MoS<sub>2</sub>). It has been expected as a candidate of flexible small quantum transistor materials<sup>8,9</sup> in post-Moore era, due to its moderate direct band gap at few layers<sup>10-12</sup> comparing to semi-metallic graphene. Until now, a variety of methods have been developed<sup>13-16</sup> to fabricate a few layers or monolayer MoS<sub>2</sub>, including mechanically exfoliation, liquid exfoliation, thermal decomposition and chemical vapour deposition (CVD). Among them, the CVD method has been demonstrated as a promising method in producing large continuous MoS<sub>2</sub> films<sup>17</sup>, thickness modulated MoS<sub>2</sub> films<sup>18,19</sup>, and even large-area and highly quality monolayer MoS<sub>2</sub> films<sup>20</sup>. In the CVD growth process, temperature, gas flow and substrate all play essential roles in determining the final film morphology, crystalline structure and quality of film. In the previous reports, the different substrates, such as amorphous SiO<sub>2</sub>/Si<sup>18,21,22</sup>, single-crystal mica<sup>19</sup> and sapphire<sup>23</sup>, were adopted in MoS<sub>2</sub> CVD growth. In these cases, the triangular MoS<sub>2</sub> films were mainly synthesized due to the little influence of substrates. The synthesis of MoS<sub>2</sub> film belongs to Van der Waals epitaxial growth and may be influenced by the symmetry of substrates. Such as, SrTiO<sub>3</sub> with quartic symmetry, has been used to synthesize MoS<sub>2</sub> dendritic flakes with three-fold symmetry<sup>6,24,25</sup>. In this regard, it is imperative to know the effect of substrate symmetry in MoS<sub>2</sub> CVD growth process.

Though there is a paper about MoS<sub>2</sub> synthesis by use of silicon carbide (SiC) as substrate, the MoS<sub>2</sub> is a vertically standing triangles, and isn't the dendritic morphology<sup>26</sup>. Here, we firstly synthesize dendritic MoS<sub>2</sub> with

<sup>1</sup>Center of Spintronics and Quantum System, State Key Laboratory for Mechanical Behavior of Materials, School of Material Science and Engineering, Xian Jiaotong University, Xi'an, 710049, China. <sup>2</sup>National Laboratory of Solid State Microstructures and Department of Materials Science and Engineering, Nanjing University, Nanjing, 210093, China. <sup>3</sup>Department of Applied Physics, School of Science, Xi'an Jiaotong University, Xi'an, 710049, China. <sup>4</sup>Department of Optical Information Science and Technology, School of Science, Xi'an Jiaotong University, Xi'an, 710049, China. Correspondence and requests for materials should be addressed to M.X. (email: [xiamg@mail.xjtu.edu.cn](mailto:xiamg@mail.xjtu.edu.cn)) or Z.G. (email: [zbg@nju.edu.cn](mailto:zbg@nju.edu.cn))

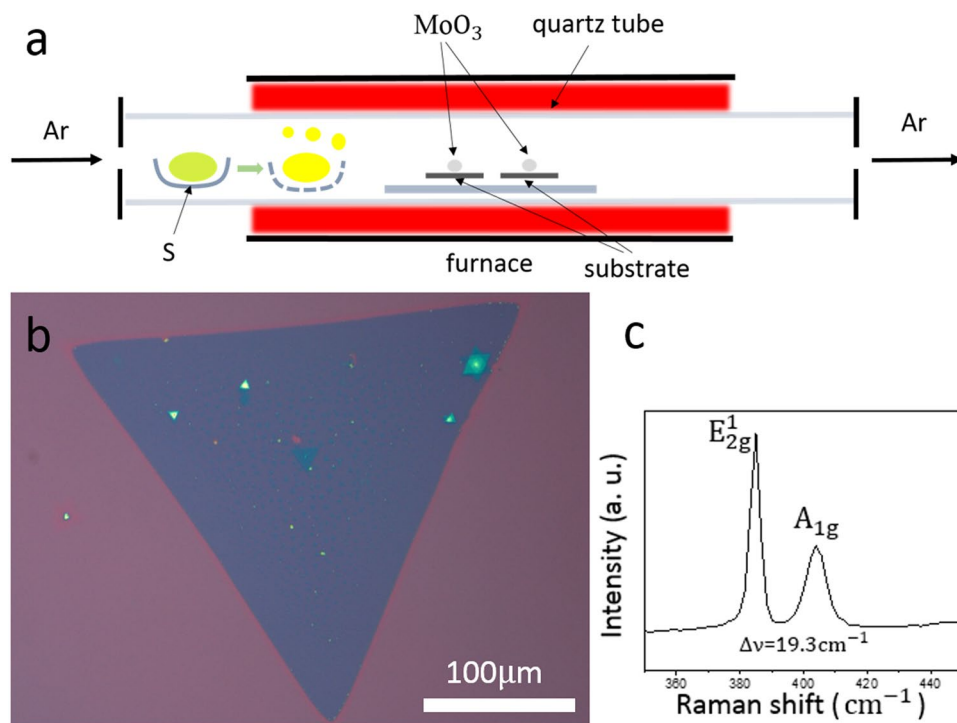


**Figure 1.** (a) The corresponding locations of sulphur, MoO<sub>3</sub>, and substrate are indicated in a single-temperature-zone CVD system. (b) Optical image of MoS<sub>2</sub> triangle film on SiO<sub>2</sub> substrate. (c) Relative Raman peak intensities and peak positions of the E<sub>2g</sub><sup>1</sup> and A<sub>1g</sub> modes of the MoS<sub>2</sub> triangle.

six-fold symmetry and two-fold symmetry by use of single crystal SiC as a substrate, which is also different from that with three-fold symmetry on the SrTiO<sub>3</sub><sup>6,24,25</sup>. To explain the novel morphology formation, we adopt the diffusion limited aggregation (DLA) to reveal the reaction process of initial crystal growth. It has been observed that the symmetry of the single crystal SiC substrate played an irreplaceable role in dendritic crystal formation. In order to show the dominant role of the substrate symmetry further, we etched the SiC substrate into the grooves to break the substrate original six-fold symmetry artificially. This resulted in the cross-shaped dendritic MoS<sub>2</sub> films, which is different from six-fold symmetry previously. This work provides not only one possibility of artificial induction of crystal growth orientation through controlling the substrate symmetry, but also provides a case for deeply understanding the detailed dynamics in non-equilibrium crystal growth of two-dimensional materials.

## Results and Discussion

Before researching the substrate effect on film growth properties in MoS<sub>2</sub> CVD synthesis, we used the common silicon substrate with 285 nm insulating SiO<sub>2</sub> as a monitor of growth conditions. Through optimizing the growth conditions, ~300 μm triangular MoS<sub>2</sub> crystal (Fig. 1b) has been achieved in a CVD setup (Fig. 1a) at atmospheric pressure. Raman spectroscopy was performed on this sample and relative Raman peak intensities and peak positions of the E<sub>2g</sub><sup>1</sup> and A<sub>1g</sub> modes of the MoS<sub>2</sub> have been acquired. As shown in Fig. 1c, this MoS<sub>2</sub> crystal grown on SiO<sub>2</sub> shows the frequency difference ( $\Delta\nu$ ) of 19.3 cm<sup>-1</sup>, less than 20 cm<sup>-1</sup>, which is a monolayer in nature<sup>27-30</sup>. Additionally, many secondary nucleation sites on top of the big triangle monolayer film can be easily observed, which is similar to other reports<sup>31</sup>. However, their formation mechanism in the final film morphology is beyond this paper's scope.

The MoS<sub>2</sub> crystal grown on SiC substrate has shown clearly dendritic form as shown in Fig. 2, instead of compact triangular structure obtained on SiO<sub>2</sub>/Si substrate. The optical image recorded over a large region with plentiful MoS<sub>2</sub> dendritic crystal, like snowflakes, on the SiC substrate, as shown in Fig. 2a. Most of the islands' sizes are around 100 μm. The area within the red rectangular region of Fig. 2a was zoomed in and shown in Fig. 2b. In the image, it can be observed clearly that two hexagonal dendritic crystals have same six-fold symmetric backbones, extending with many hierarchical branches harbouring similar angle. In some regions on SiC wafer, the backbones only extend a few secondary branches, while in other regions, the continuous films were observed, which may be due to different local growth conditions. The inset in Fig. 2b is the MoS<sub>2</sub> flakes grown on SiO<sub>2</sub> substrate in the same batch growth as a comparison. The scale bar is 10 μm. The X-ray photoelectron spectroscopy (XPS) data of the dendritic crystals grown on SiC reveals the occurrence of Mo 3d<sup>3/2</sup> and 3d<sup>5/2</sup> states at binding energies of 232.7 eV and 229.6 eV, and 2p<sup>1/2</sup> and 2p<sup>3/2</sup> states of S at 163.7 eV and 162.4 eV respectively (Fig. 2e). These are typical signs for MoS<sub>2</sub> films<sup>32-34</sup>. To characterize the flakes' structure in more details, a high resolution scanning electron microscope (SEM) image was taken in Fig. 2c. Similar to the optical images, it also shows the backbones and many hierarchical branches. While, there is no any hierarchical branch in some backbones. From the morphology comparison, we can found clearly that the MoS<sub>2</sub> grown on SiO<sub>2</sub> in the same batch growth is the compact

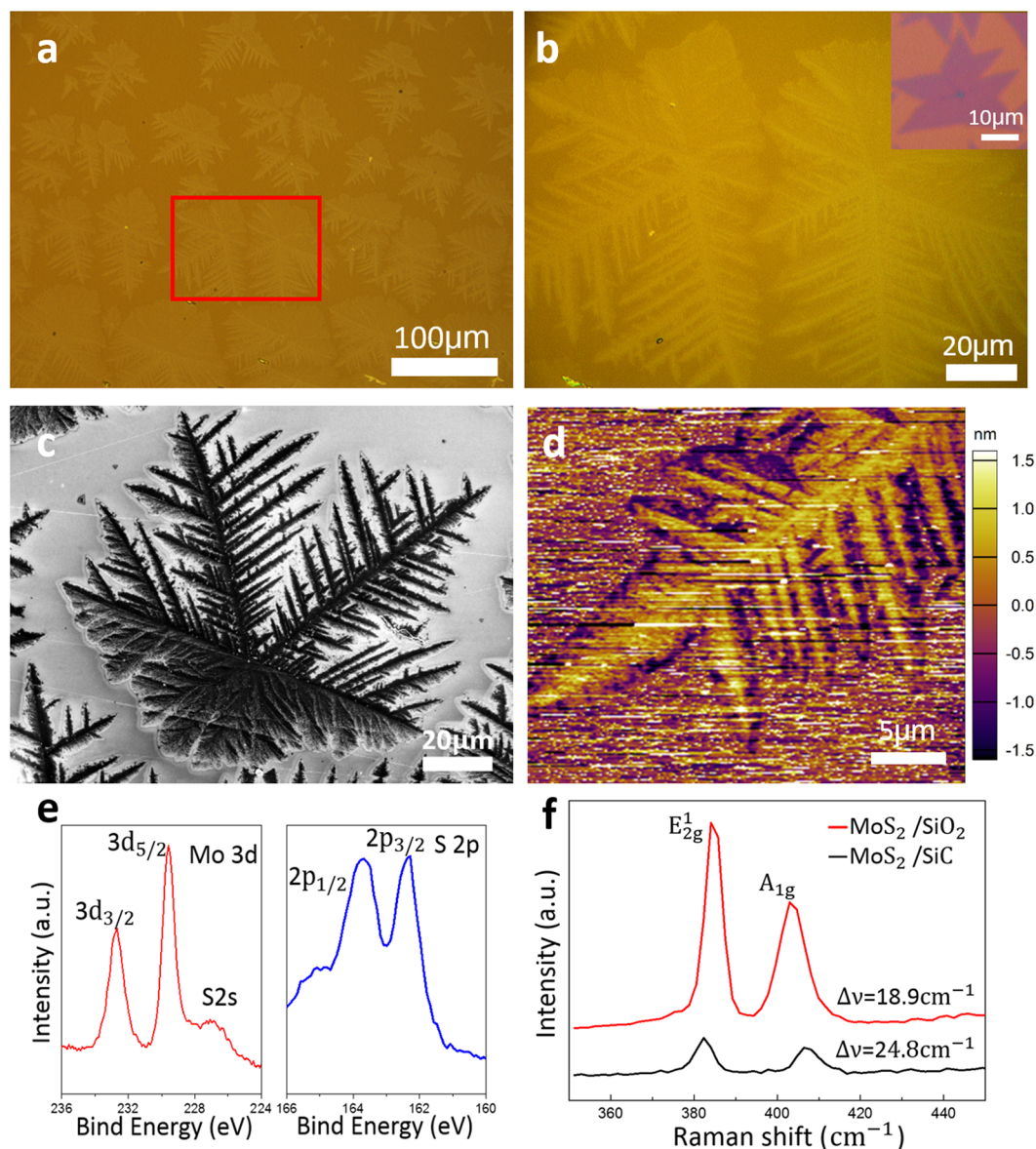


**Figure 2.** CVD synthesis, XPS and Raman characterizations of dendritic MoS<sub>2</sub> on SiC. **(a,b)** Optics images in different amplification showing the dendritic MoS<sub>2</sub> flakes grown on SiC. The inset in **(b)** is the MoS<sub>2</sub> flakes grown on SiO<sub>2</sub> substrate of the same batch growth as a comparison. **(c,d)** SEM and AFM images revealing the details of snow-like MoS<sub>2</sub> flakes. **(e)** X-ray photoemission spectroscopy (XPS) data of MoS<sub>2</sub> on SiC. **(f)** Raman spectroscopy data of MoS<sub>2</sub> on SiC and SiO<sub>2</sub>.

triangle crystal, which suggests that the substrate affects the final film morphology of MoS<sub>2</sub>. Even though various shapes with or without additional branches can be observed, all of them exhibit the basic triangle shapes or their combining forms, which is similar to previous reports of MoS<sub>2</sub> grown on SiO<sub>2</sub>/Si substrate<sup>20,21,35</sup>.

Micro-Raman spectroscopy has been widely utilized to characterize the 2D materials. The native MoS<sub>2</sub> grown on SiC and SiO<sub>2</sub> was scanned by 518 nm wavelength laser, and their Raman spectra were shown in Fig. 2f. It can be observed that two samples grown on SiC and SiO<sub>2</sub> all show typical characteristic Raman modes of MoS<sub>2</sub>, E<sub>2g</sub><sup>1</sup> and A<sub>1g</sub> peaks, around 380 and 402 cm<sup>-1</sup>. Their frequency difference ( $\Delta\nu$ ) for the MoS<sub>2</sub> on SiO<sub>2</sub> is 18.9 cm<sup>-1</sup> which is a monolayer in nature<sup>27-30</sup>. But their frequency difference is 24.8 cm<sup>-1</sup> in MoS<sub>2</sub> on SiC, corresponding to a thicker film. The Atomic Force Microscope (AFM) image (Fig. 2d) reveals more details about the morphology and thickness of the snow-like MoS<sub>2</sub> dendrite. It indicates that the thickness of the dendritic MoS<sub>2</sub> flakes is at most 3 nm, approximate 5 layers.

The two-dimensional crystal growth mechanism of MoS<sub>2</sub> can usually be described by following process: 1) nucleation, 2) diffusion and growth, 3) formation of crystals. The symmetry of substrate dominates the nucleation process and plays a critical role in determining whether a compact or fractal growth. In other words, the substrate with triangular or hexagonal geometry is easier to have extended fractal growth than square lattice<sup>36-38</sup>. To obtain the symmetry of the MoS<sub>2</sub> film morphology in more detail via CVD growth method, we carried out the angular



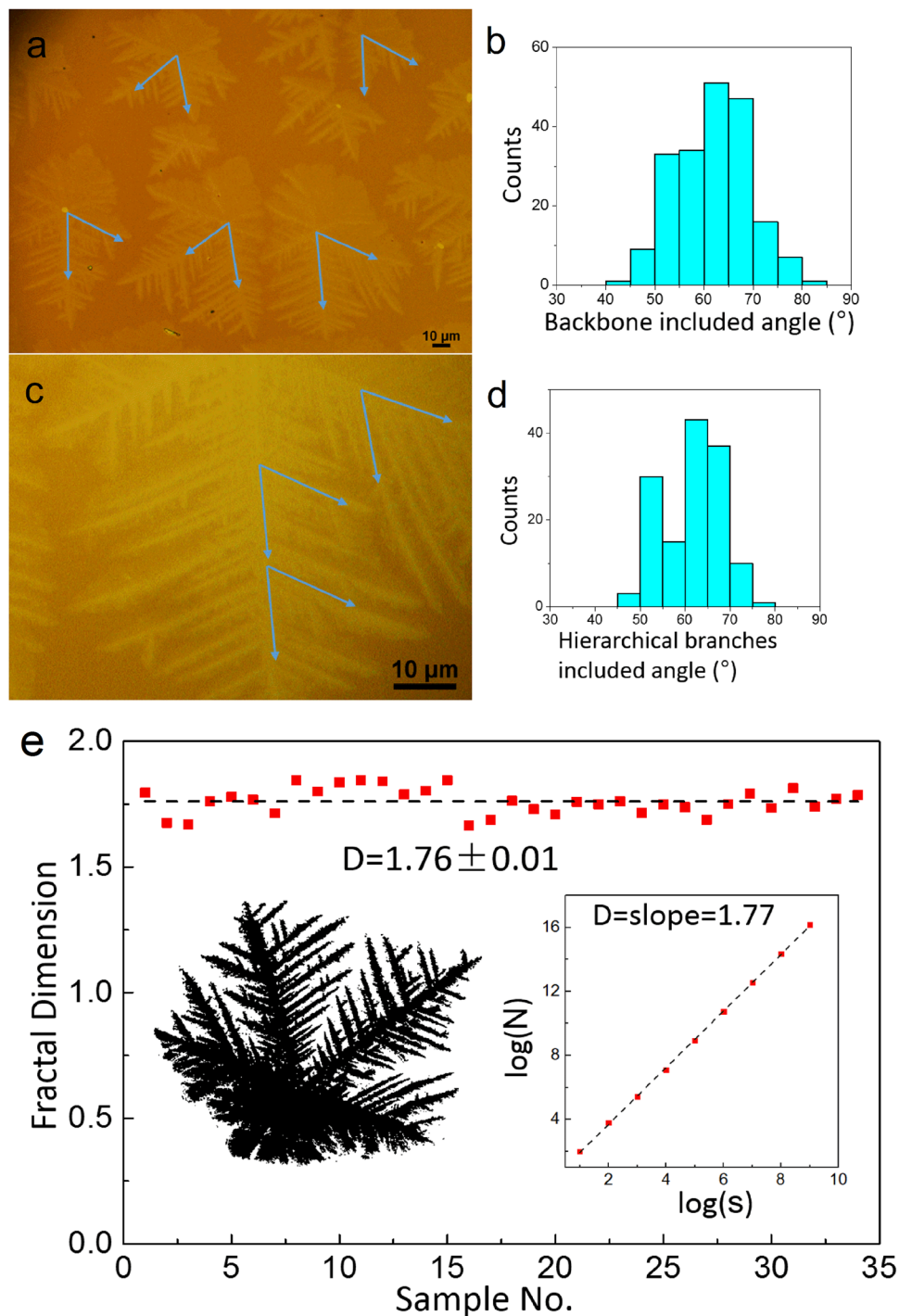


**Figure 3.** Statistics of the backbones and the hierarchical branches angles, and Fractal dimension calculation of  $\text{MoS}_2$  dendrites on SiC (0001). (a) Optical image of the  $\text{MoS}_2$  dendrites featured with  $60^{\circ}$  included angles backbones (highlighted with blue arrows). (b) Statistics of the two backbone included angles for 200 flakes. (c) Magnified optical image of hierarchical branches showing with  $60^{\circ}$  included angles. (d) Statistics of hierarchical branches included angles for 140 flakes. (e) Statistics for 34 snow-like  $\text{MoS}_2$  dendrites (Left inset: contrast-enhanced SEM image of a typical snow-like  $\text{MoS}_2$  dendrite; Right inset: box-counting estimation of the fractal dimension for the left flake).

distribution of the dendritic morphology of  $\text{MoS}_2$  on SiC statistically. The orientation of backbones of dendrites were illustrated by the blue arrows, between which are  $60^{\circ}$  angles usually, shown in Fig. 3a. And the angle between the subsequent hierarchical branches and the main backbones is also about  $60^{\circ}$ , seen in Fig. 3c. It has been confirmed that both angle distributions are centred at  $60^{\circ}$ , shown in Figs 3b and d, by the angle statistics from 200 flakes of backbone and 140 flakes of hierarchical branches.



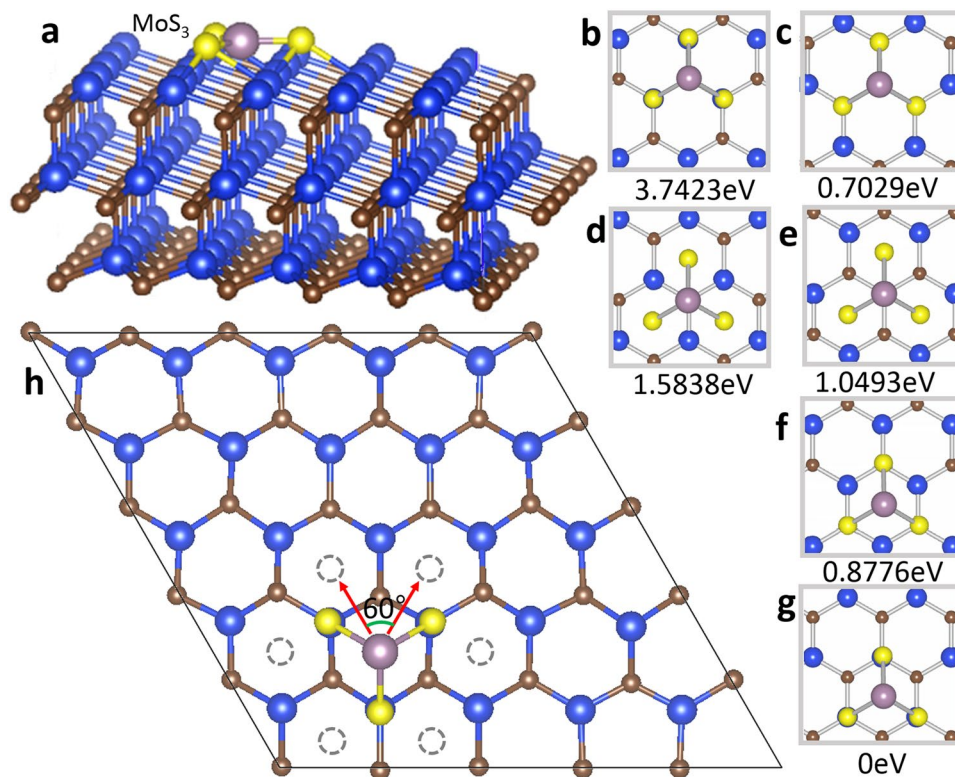


**Figure 4.** Density functional theory (DFT) calculations of assumed  $\text{MoS}_3$  monomer precursor on Si-terminated SiC surface. **(a)** Actual calculation unit cell with a  $\text{MoS}_3$  molecule and 10 Å vacuum space along the z direction. Blue, brown, light brown, and yellow balls denote the Si, C, Mo and S atoms, respectively. **(b–g)** Six modes of  $\text{MoS}_3$  molecule adopted on different position on SiC surface. Corresponding negative bonding energy were showed under the images respectively. **(h)** The most stable adsorption configuration (Fig. 4g) for a  $\text{MoS}_3$  monomer on SiC (0001). The red arrow reveals schematic illustration of the probable diffusion pathways for a  $\text{MoS}_3$  monomer on SiC (0001). Dotted circles represent the six closet adsorption sites.

In order to describe the morphology of  $\text{MoS}_2$  flakes in more detail, the fractal dimension is calculated statistically, presented in Fig. 3e. Thirty-four flakes on the same sample was comprehensively estimated by use of a standard box-counting evaluation. The left inset is a contrast-enhanced SEM image of a typical snow-like  $\text{MoS}_2$  dendrite crystal; while the right inset is a box-counting estimation of the fractal dimension for the left flake. These flakes exhibit an average fractal dimension of  $1.76 \pm 0.01$ . This fractal dimension is in good agreement with the classical DLA dimension of 1.66. This also demonstrates the natural fractal property of the snow-like  $\text{MoS}_2$  dendrite indirectly.

Whether the six-fold symmetry observed in the dendritic morphology is influenced by the substrate surface symmetry or not? In order to reply the question, the density functional theory (DFT) calculations were performed. The binding energies of a  $\text{MoS}_x$  monomer on various configurations on the Si-terminated SiC (0001) surface are computed. Here the molecular  $\text{MoS}_3$  was assumed to be the representative monomer precursor for the final  $\text{MoS}_2$  film because it is the dominate phase in the low-temperature and excess sulphur regime, according to the Mo-S phase diagram<sup>39</sup>. In the DFT model, the SiC substrate with Si-terminated surface was modelled by a three layers  $5 \times 5$  superlattice with total 150 atoms as shown in Fig. 4a. And a vacuum space of 10 Å along the direction perpendicular to the surface was used to avoid interactions between adjacent layers. Six absorption sites of  $\text{MoS}_3$  molecule on SiC surface were calculated and the corresponding bonding energy to the lowest energy mode (Fig. 4g) were shown under each image, respectively (Fig. 4b–g). Note that the most energetically favourable adsorption site for  $\text{MoS}_3$  is for the Mo atom sitting above the centre of the hexagonal lattice while the S atom locating on top of Si atoms, as shown in Fig. 4g, where the unsaturated S and Si atoms could form effective bonding with each other. Because of the natural hexagonal symmetry of SiC, it is obvious that there are six closest equal adsorption sites near the energetically favourable adsorption site and six preferential equal diffusion pathways oriented 60 degree to each other as shown in Fig. 4h. This is in agreement well with the statistical results about the 60 degree angle between the backbones of dendritic  $\text{MoS}_2$  flakes.

The formation of the dendritic morphology could be inferred by the DLA mechanism<sup>36,40,41</sup>. When the  $\text{MoS}_3$  molecule was adsorbed onto substrate, it might have some energy to move around on the surface. According to our calculation, the molecule prefer the position energetically on where the Mo atom is rest upon the centre of the hexagonal lattice because this configuration has the lowest binding energy, and thus it serves as an nucleation site. This nucleation on SiC substrate doesn't like the previous  $\text{SiO}_2$ , sapphire and Mica substrate, on which it prefers to happen on impurity or defects.

Subsequent adsorbed atoms (ad-atoms) deposit onto the substrate and diffuse in a certain way. They might hopping around onto different sites but the configuration with Mo sitting at the centre of Si-C hexagon is energetically favoured and will serve with stronger sticking coefficient. When the ad-atoms encounter those nucleation centres, three situations might happen, which is determined by the difference between particle diffusing and bonding energy. The first is that the particles don't diffuse and become attached to the nucleation centre and being part of cluster. The second is that the ad-atoms continue walking on the substrate surface and not adsorbed with any cluster. The third is that they become one part of the cluster, but continue to diffuse along the cluster edges. With the increasing of the cluster size, more and more ad-atoms have the chance to meet the island and the cluster continues to grow. It suggests that the first and the second situations would always happen until there are no ad-atom left on the surface. What is interesting is the third case, the ad-atoms with proper energy diffuse limitedly along the edge so that they couldn't cross the corner to make the edge relaxing and new corners would be generated. Subsequent ad-atoms follow the former atoms and more edge are generated. With the increasing of edges and corners, the ad-atoms have less chance to fill the vacancy sites and relax along the edge<sup>36,37</sup>. In our case, it suggests that because the SiC substrate has strong dangling bond<sup>42,43</sup>, comparing to amorphous SiO<sub>2</sub>, the MoS<sub>x</sub> molecule need higher energy to diffuse along the edge so that it prefers to stick to the nucleation sites, according to the DFT calculation, leading to more edges and insufficient edges relaxation once they encounter a cluster. In a word, whether precursors could diffuse freely or form dendrite in the substrate surface depends on the competition among its energy, the temperature, the interaction between the precursor and the substrate, and the interaction between the precursor and the established island or cluster. In our case, since the strong dangling bond of the SiC substrate, the more compact dendritic MoS<sub>2</sub> film was formed and its fractal dimension is bigger than the classical one. Furthermore, due to the natural hexagonal symmetry of those nucleation sites on SiC (0001) surface, the dendritic edges prefer arranging along the centre of hexagonal Si-C ring to form a unique dendritic shape with six-fold symmetry. About the dendritic shape with six-fold symmetry in two dimension, there is another material, graphene dendritic on copper<sup>44</sup>. MoS<sub>2</sub> dendritic with six-fold symmetry is different from the graphene one because the former owns three atoms layer structure, while the latter is only one atom layer structure. The most important is that the morphology of graphene dendritic is determined by itself symmetry, not by the substrate, copper. MoS<sub>2</sub> dendritic is fully determined by the symmetry of the SiC substrate<sup>44</sup>. Furthermore, from DLA mechanism, we can know that another energy term in first principle calculation, a stick potential barrier works in MoS<sub>2</sub> dendritic growth.

To further demonstrate that the SiC surface symmetry determines the final dendritic morphology of MoS<sub>2</sub> film in CVD, we created an artificial surface structure on substrate to change the nucleation sites symmetry. The chemical etching process is presented to accomplish the aim. Prior to MoS<sub>2</sub> growth, the SiC substrate was immersed in hydrofluoric acid (HF, 1%) for 24 h before washing. Artificial grooves with about 3 nm depth and 100 nm width was created, shown in Fig. 5e. The MoS<sub>2</sub> film grown on the etched SiC shows a cross-type dendrite with two-fold symmetry, as shown by the optical and SEM images of Figs 5a–c. Most of the island's size are around 20 μm, much smaller than 100 μm crystals on native SiC. As a comparison, the MoS<sub>2</sub> on SiO<sub>2</sub> under the same batch growth is shown in the inset of Fig. 5b (the scale bar is 10 μm). By comparing these images, it is obvious that the new two-fold symmetry MoS<sub>2</sub> dendrite is different from the six-fold MoS<sub>2</sub> on native SiC and from the compact crystal on SiO<sub>2</sub>. Furthermore, the orientation of the two-fold dendrites are aligned with the long axis along roughly the same direction of the grooves. This has been suggested by the statistics of main axis orientation for the dendritic flakes, seen in Fig. 5d. To confirm the crystal grown on etched SiC is still MoS<sub>2</sub>, XPS was also collected, and the result is shown by Fig. 5f: the occurrence of Mo 3d<sup>3/2</sup> and 3d<sup>5/2</sup> states at binding energies of 232.7 eV and 229.6 eV, and 2p<sup>1/2</sup> and 2p<sup>3/2</sup> states of S at 163.7 eV and 162.4 eV, which are typical signs for MoS<sub>2</sub> film. Furthermore, the SEM and AFM images have shown more morphology details (Figs 5c,e). Wavy MoS<sub>2</sub> flakes with groove arrays can be observed, which indicates again that the long axis of cross-type dendrite is along the groove direction. Comparing to the six-fold MoS<sub>2</sub>, the fractal dimension of two-fold MoS<sub>2</sub> is around 1.83 by statistics for twenty-one cross-type dendritic MoS<sub>2</sub> flakes (Fig. 5g). The fractal dimension is slightly bigger than that of the six-fold one, so we can infer the two-fold dendritic MoS<sub>2</sub> is more compact than six-fold one. It is attributed to a potential barrier. On the etched SiC substrates, the precursor should overcome an additional potential barrier across artificial groove arrays to diffuse on the surface, than on the native SiC substrate.

The details of the two-fold dendrite growth should be further understood under DLA mechanism as well. On the etched SiC substrates, the artificial grooves create an anisotropy diffusion potential barrier, which induces an anisotropy sticking energy. Therefore, the energy should hinder diffusion of the precursor molecule across the groove direction, comparing to direction along the groove. During growth, the ad-atoms have much higher probability stuck to those sites at edge of grooves, causing faster growth of crystal along the groove direction than across it. Comparing the native SiC substrate, the hexagonal symmetry of the diffusion paths have been broken, which are replaced by insufficient diffusion across the grooves and faster diffusion along to the grooves. This suggests that two orthometric pathways in the etched SiC substrate lead to the novel cross-type shape dendrites under the DLA mechanism. Therefore, we conclude that the dendritic morphology of MoS<sub>2</sub> grown on SiC substrate can be modified to the desired morphology through artificially constructing special substrate surface in the CVD growth process. This also inspires us to explore novel symmetry of dendrite, different from its natural, by the use of special substrate or the special symmetry structure on surface of substrate.

## Conclusion

In summary, we have achieved the MoS<sub>2</sub> dendritic in CVD on single-crystal SiC. The obtained MoS<sub>2</sub> flakes show a special snow-shaped dendritic morphology with six-fold symmetry, in contrast with the traditional sharp-edged triangular compact flakes grown on conventional SiO<sub>2</sub> substrate. The growth dynamics of this morphology can be readily explained by the classical Diffusion-Limited-Aggregation mechanism. Additionally, we find the intrinsic lattice symmetry of the SiC substrate can be broken by etching, and obtained cross-shaped dendritic MoS<sub>2</sub> films,

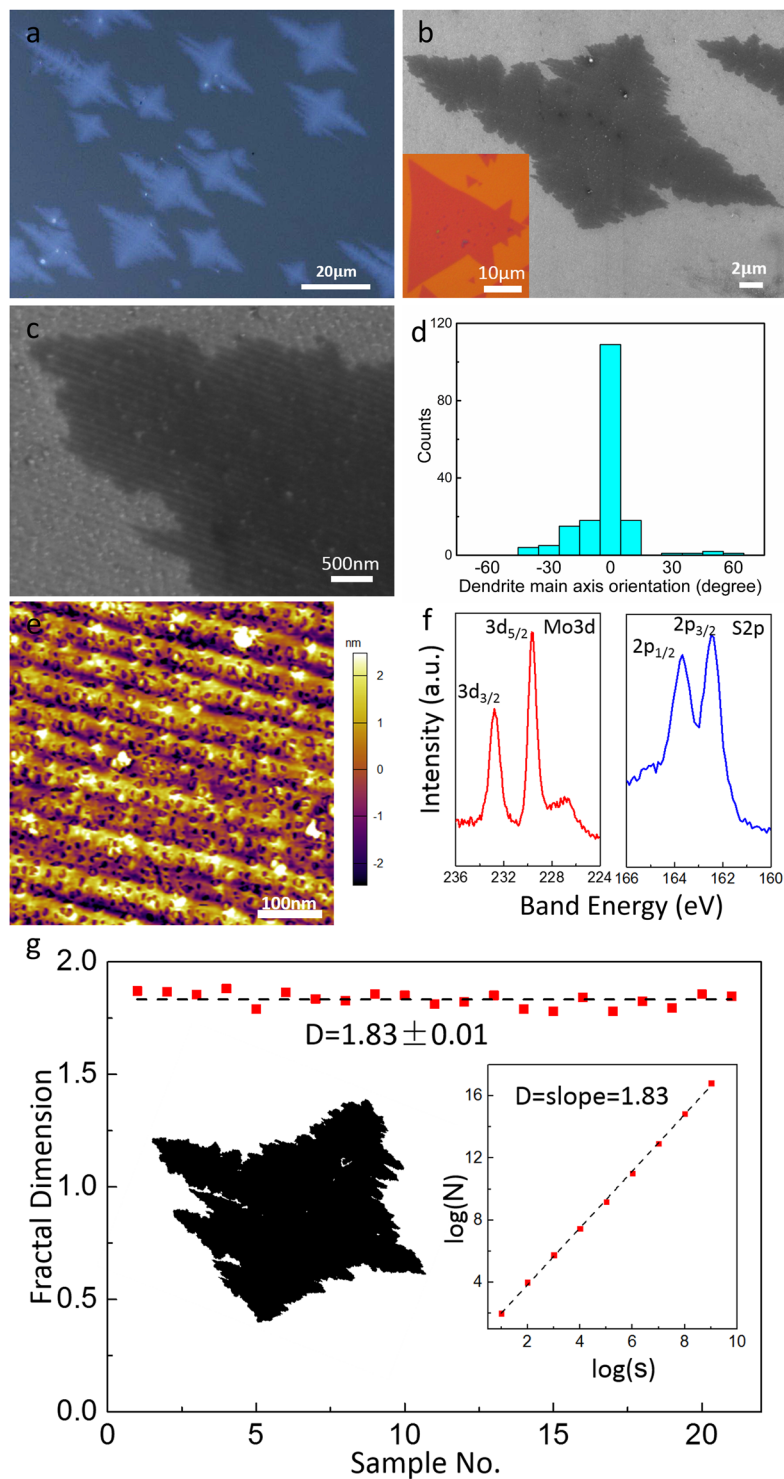


**Figure 5.** CVD synthesis and Fractal dimension calculation of MoS<sub>2</sub> on etched SiC and SiO<sub>2</sub>. (a–c) Optics and SEM images show the cross-type MoS<sub>2</sub> flakes on etched SiC in different magnification. The inset in (b) shows the MoS<sub>2</sub> flakes grown on SiO<sub>2</sub> substrate in the identical furnace as comparison. (c) SEM images showing the MoS<sub>2</sub> polycrystalline on etched SiC in a different scale. The inset is the left partial enlarged view of the dendritic flake. (d) Statistics of the dendrite main axis orientation angles for 140 flakes. (e) The AFM image showed the groove of MoS<sub>2</sub> on etched SiC. (f) XPS data of MoS<sub>2</sub> on etched SiC. (g) Statistics for 21 cross-type dendritic MoS<sub>2</sub> flakes (Left inset: contrast-enhanced SEM image of a typical cross-type MoS<sub>2</sub> dendrite; Right inset: box-counting estimation of the fractal dimension for the left flake).



further suggesting that the substrate plays a crucial role in dendritic growth process. Furthermore, by comparing the two kind of fractal dimension of dendrite with the classical one, we found that the substrate effect on the MoS<sub>2</sub> dendrite would be enhanced due to the additional potential barrier. This work could contribute to further in-depth understanding of the detailed dynamics in non-equilibrium crystal growth of two-dimensional materials and provides one possibility of artificially inducing the growth orientation of crystals through controlling the substrate surface symmetry.

## Methods

The MoS<sub>2</sub> flakes were produced utilizing the facile CVD technique. High purity MoO<sub>3</sub> (99.5%, Alfa Aesar) and sulphur powder (99.9%, Alfa Aesar) were used as precursors. The MoO<sub>3</sub> powder (less than 1 mg) was sowed directly on the substrate which was placed at the centre of a 4-inch diameter CVD furnace by a flat quartz board. The sulphur powder was kept in a quartz boat placed upstream at a lower temperature zone out of the furnace. The distance between sulphur boat and the substrate was maintained to be ~50 cm.

We used single crystal 4H-SiC wafers as substrates, where the crystal orientation is <0001> and 4° toward <112(-)0>. All substrates were first immersed in a freshly prepared piranha solution (H<sub>2</sub>SO<sub>4</sub>:H<sub>2</sub>O<sub>2</sub>, 7:3) for 24 h. Then they were washed with de-ionized (DI) water two times, repeatedly, and sonicated in acetone and subsequently in isopropyl alcohol (IPA) for 5 min each before blow-dried by nitrogen. In addition, when it needs etching, the SiC substrate was etched by immersing in hydrofluoric acid (HF, 1%) for 24 h. And all other processes were then completed repeatedly.

Prior to the growth, the quartz tube of CVD furnace was cleaned completely. The furnace was then heated to 300 °C for 60 min under Ar gas. Then the temperature was ramped up to 700 °C at a rate of 10 °C/min. At this stage, the sulphur boat was pushed into heated zone to a suitable position. Then the furnace was kept in 700 °C for 20 min before cooled naturally. In the whole process, the gas flow rate was kept at 500 sccm.

The SEM measurements were done using a Zeiss Ultra 55 FESEM system. The Raman spectroscopy were executed at room temperature in back scattering geometry using a Renishwa's Invia confocal Raman spectrometer with argon ion laser (514 nm excitation). The size of the focused laser spot on the sample was ~1 μm. The laser power was kept at 12 μW for all the measurements. The X-ray photoelectron spectroscopy (XPS Thermo Fisher K-Alpha) measurements were done with standard Al K<sub>α</sub> (1486.7 eV) x-ray source. The binding energies were calibrated with respect to the signal from the adventitious carbon (binding energy = 284.5 eV). AFM measurement was performed on an Asylum Research Company Cypher-ES system.

## References

- Wang, Q. H., Kalantar-Zadeh, K., Kis, A., Coleman, J. N. & Strano, M. S. Electronics and optoelectronics of two-dimensional transition metal dichalcogenides. *Nat. Nanotechnol.* **7**, 699–712 (2012).
- Baugher, B. W. H., Churchill, H. O. H., Yang, Y. & Jarillo-Herrero, P. Optoelectronic devices based on electrically tunable p-n diodes in a monolayer dichalcogenide. *Nat. Nanotechnol.* **9**, 262–267 (2014).
- Ugeda, M. M. *et al.* Giant bandgap renormalization and excitonic effects in a monolayer transition metal dichalcogenide semiconductor. *Nat. Mater.* **13**, 1091–1095 (2014).
- Pumera, M., Sofer, Z. & Ambrosi, A. Layered transition metal dichalcogenides for electrochemical energy generation and storage. *J. Mater. Chem. A* **2**, 8981–8987 (2014).
- Bonaccorso, F. *et al.* Graphene, related two-dimensional crystals, and hybrid systems for energy conversion and storage. *Science* **347**, 1246501 (2015).
- Zhang, Y. *et al.* Dendritic, transferable, strictly monolayer MoS<sub>2</sub> flakes synthesized on SrTiO<sub>3</sub> single crystals for efficient electrocatalytic applications. *ACS nano* **8**, 8617–8624 (2014).
- Chhowalla, M. & Amaratunga, G. A. J. Thin films of fullerene-like MoS<sub>2</sub> nanoparticles with ultra-low friction and wear. *Nature* **407**, 164–167 (2000).
- Ponomarev, E., Gutierrez-Lezama, I., Ubrig, N. & Morpurgo, A. F. Ambipolar light-emitting transistors on chemical vapor deposited monolayer MoS<sub>2</sub>. *Nano Lett.* **15**, 8289–8294 (2015).
- Sangwan, V. K. *et al.* Gate-tunable memristive phenomena mediated by grain boundaries in single-layer MoS<sub>2</sub>. *Nat. Nanotechnol.* **10**, 403–406 (2015).
- Splendiani, A. *et al.* Emerging photoluminescence in monolayer MoS<sub>2</sub>. *Nano Lett.* **10**, 1271–1275 (2010).
- Mak, K. F., Lee, C., Hone, J., Shan, J. & Heinz, T. F. Atomically thin MoS<sub>2</sub>: a new direct-gap semiconductor. *Phys. Rev. Lett.* **105**, 136805 (2010).
- Liu, Q. *et al.* Tuning electronic structure of bilayer MoS<sub>2</sub> by vertical electric field: a first-principles investigation. *J. Phys. Chem. C* **116**, 21556–21562 (2012).
- Wang, F. *et al.* Recent advances in transition-metal dichalcogenide based nanomaterials for water splitting. *Nanoscale* **7**, 19764–19788 (2015).
- Gan, X., Zhao, H. & Quan, X. Two-dimensional MoS<sub>2</sub>: A promising building block for biosensors. *Biosens. Bioelectron.* **89**, 56–71 (2016).
- Tan, C. & Zhang, H. Two-dimensional transition metal dichalcogenide nanosheet-based composites. *Chem. Soc. Rev.* **44**, 2713–2731 (2015).
- Coleman, J. N. *et al.* Two-dimensional nanosheets produced by liquid exfoliation of layered materials. *Science* **331**, 568–571 (2011).
- Liu, K. K. *et al.* Growth of large-area and highly crystalline MoS<sub>2</sub> thin layers on insulating substrates. *Nano Lett.* **12**, 1538–1544 (2012).
- Choudhary, N., Park, J., Hwang, J. Y. & Choi, W. Growth of large-scale and thickness-modulated MoS<sub>2</sub> nanosheets. *ACS Appl. Mater. Inter.* **6**, 21215–21222 (2014).
- Xu, Y. Y. *et al.* Layer-controlled large area MoS<sub>2</sub> layers grown on mica substrate for surface-enhanced Raman scattering. *Appl. Surf. Sci.* **357**, 1708–1713 (2015).
- van der Zande, A. M. *et al.* Grains and grain boundaries in highly crystalline monolayer molybdenum disulphide. *Nat. Mater.* **12**, 554–561 (2013).
- Ji, Q., Zhang, Y., Zhang, Y. & Liu, Z. Chemical vapour deposition of group-VIB metal dichalcogenide monolayers: engineered substrates from amorphous to single crystalline. *Chem. Soc. Rev.* **44**, 2587–2602 (2015).
- Lin, Z. *et al.* Controllable growth of large-size crystalline MoS<sub>2</sub> and resist-free transfer assisted with a Cu thin film. *Sci. Rep.* **5**, 18596 (2015).

23. Wu, C. R. *et al.* Multilayer MoS<sub>2</sub> prepared by one-time and repeated chemical vapor depositions: anomalous Raman shifts and transistors with high ON/OFF ratio. *J. Phys. D: Appl. Phys.* **48**, 435101 (2015).
24. Ji, Q. *et al.* Morphological engineering of CVD-grown transition metal dichalcogenides for efficient electrochemical hydrogen evolution. *Adv. Mater.* **28**, 6207–6212 (2016).
25. Zhang, Y. *et al.* Monolayer MoS<sub>2</sub> dendrites on a symmetry-disparate SrTiO<sub>3</sub> (001) substrate: formation mechanism and interface interaction. *Adv. Fun. Mater.* **26**, 3299–3305 (2016).
26. Lan, F. F. *et al.* Synthesis of Vertically Standing MoS<sub>2</sub> Triangles on SiC. *Sci. Rep.* **6**, 31980 (2016).
27. Windom, B. C., Sawyer, W. G. & Hahn, D. W. A Raman spectroscopic study of MoS<sub>2</sub> and MoO<sub>3</sub>: applications to tribological systems. *Tribol. Lett.* **42**, 301–310 (2011).
28. Hussain, S. *et al.* Controlled synthesis and optical properties of polycrystalline molybdenum disulfide atomic layers grown by chemical vapor deposition. *J. Alloys Compd.* **653**, 369–378 (2015).
29. Li, H. *et al.* From bulk to monolayer MoS<sub>2</sub>: evolution of Raman scattering. *Adv. Fun. Mater.* **22**, 1385–1390 (2012).
30. Najmaei, S., Liu, Z., Ajayan, P. M. & Lou, J. Thermal effects on the characteristic Raman spectrum of molybdenum disulfide (MoS<sub>2</sub>) of varying thicknesses. *Appl. Phys. Lett.* **100**, 013106 (2012).
31. Han, G. H. *et al.* Seeded growth of highly crystalline molybdenum disulphide monolayers at controlled locations. *Nat. Com.* **6**, 6128 (2015).
32. Qiu, D., Lee, D. U., Pak, S. W. & Kim, E. K. Structural and optical properties of MoS<sub>2</sub> layers grown by successive two-step chemical vapor deposition method. *Thin Solid Films* **587**, 47–51 (2015).
33. Yang, Z. *et al.* Realization of high Curie temperature ferromagnetism in atomically thin MoS<sub>2</sub> and WS<sub>2</sub> nanosheets with uniform and flower-like morphology. *Nanoscale* **7**, 650–658 (2015).
34. Shi, J. *et al.* Monolayer MoS<sub>2</sub> growth on Au foils and on-site domain boundary imaging. *Adv. Fun. Mater.* **25**, 842–849 (2015).
35. Wang, S. *et al.* Shape evolution of monolayer MoS<sub>2</sub> crystals grown by chemical vapor deposition. *Chem. Mater.* **26**, 6371–6379 (2014).
36. Zhang, Z. & Lagally, M. G. Atomistic processes in the early stages of thin-film growth. *Science* **276**, 377–383 (1997).
37. Zhang, Z., Chen, X. & Lagally, M. G. Bonding-geometry dependence of fractal growth on metal surfaces. *Phys. Rev. Lett.* **73**, 1829–1832 (1994).
38. Ghosh, A., Batabyal, R., Das, G. P. & Dev, B. N. An extended fractal growth regime in the diffusion limited aggregation including edge diffusion. *AIP Adv.* **6**, 015301 (2016).
39. Feldman, Y., Wasserman, E., Srolovitz, D. J. & Tenne, R. High-rate, gas-phase growth of MoS<sub>2</sub> nested inorganic fullerenes and nanotubes. *Science* **267**, 222 (1995).
40. Witten, T. A. & Sander, L. M. Diffusion-limited aggregation, a kinetic critical phenomenon. *Phys. Rev. Lett.* **47**, 1400–1403 (1981).
41. Honjo, H., Ohta, S. & Sawada, Y. New experimental finding in two-dimensional dendritic crystal growth. *Phys. Rev. Lett.* **55**, 841–844 (1985).
42. Starke, U. *et al.* Novel reconstruction mechanism for dangling-bond minimization: combined method surface structure determination of SiC(111)-(3 × 3). *Phys. Rev. Lett.* **80**, 758–761 (1998).
43. Bekaroglu, E., Topsakal, M., Cahangirov, S. & Ciraci, S. First-principles study of defects and adatoms in silicon carbide honeycomb structures. *Phys. Rev. B* **81**, 075433 (2010).
44. Hao, Y. F. *et al.* The Role of Surface Oxygen in the Growth of Large Single-Crystal Graphene on Copper. *Science* **342**, 720–723 (2013).

## Acknowledgements

This work is partially supported by “Shaanxi Province Science and Technology Innovation Project of China” (2015ZS-02) and that for “National Science and Technology Major Project of China” (2016YFA0300702). M. G. Xia also thanks to the supports by State Key Laboratory for Mechanical Behaviour of Materials (Grant No. 20131311), and the Fundamental Research Funds for Central Universities (2012jdgz04). Prof. Gu want to acknowledge funding from the National Natural Science Foundation of China (51672125, 51472114).

## Author Contributions

M.X., Z.G. and T.M. conceived the idea and supervised the project. D.W., T.M., G.L. and M.X. designed research method, analysed data and conducted the material growth. D.W., J.Z., C.L., and G.M. conducted the material characterization and theoretical calculation. All authors contributed to the writing and editing.

## Additional Information

**Competing Interests:** The authors declare that they have no competing interests.

**Publisher's note:** Springer Nature remains neutral with regard to jurisdictional claims in published maps and institutional affiliations.



**Open Access** This article is licensed under a Creative Commons Attribution 4.0 International License, which permits use, sharing, adaptation, distribution and reproduction in any medium or format, as long as you give appropriate credit to the original author(s) and the source, provide a link to the Creative Commons license, and indicate if changes were made. The images or other third party material in this article are included in the article's Creative Commons license, unless indicated otherwise in a credit line to the material. If material is not included in the article's Creative Commons license and your intended use is not permitted by statutory regulation or exceeds the permitted use, you will need to obtain permission directly from the copyright holder. To view a copy of this license, visit <http://creativecommons.org/licenses/by/4.0/>.

© The Author(s) 2017